SAND80-0308
Unlimited Release

A SIMPLE METHOD FOR THE CALCULATION AND USE OF CVD PHASE DIAGRAMS WITH APPLICATIONS TO THE Ti-B-Cl-H SYSTEM, 1200K - 800K

MASTER

E. Randich and T. M. Gerlach

Sandia National Laboratories

F 2900-Q(3-80)

DISTRIBUTION OF THIS DOCUMENT IS UNLIMITED

CONTENTS

DISCLAIMER

This report was prepared as an account of work sponsored by an agency of the United States Government. Neither the United States Government nor any agency thereof, nor any of their employees, makes any warranty, express or implied, or assumes any legal liability or responsibility for the accuracy, completeness, or usefulness of any information, apparatus, product, or process disclosed, or represents that its use would not infringe privately owned rights. Reference herein to any specific commercial product, process, or service by trade name, trademark, manufacturer, or otherwise, does not necessarily constitute or imply its endorsement, recommendation, or favoring by the United States Government or any agency thereof. The views and opinions of authors expressed herein do not necessarily state or reflect those of the United States Government or any agency thereof.

DISTRIBUTION OF THIS DOCUMENT IS UNLIMITED

LIST OF FIGURES

LIST OF TABLES

SAND80-0308

A SIMPLE METHOD FOR THE CALCULATION AND USE OF CVD PHASE DIAGRAMS WITH APPLICATIONS TO THE Ti-B-Cl-H SYSTEM, 1200K - 800K

E. Randich and T. M. Gerlach
Sandia Laboratories
Albuquerque, New Mexico 87185

ABSTRACT

A simple method for calculating multi-component gas-solid equilibrium phase diagrams for chemical vapor deposition (CVD) systems is presented. The method proceeds in three steps: determination of stable solid assemblages, evaluation of gas-solid stability relations, and calculation of conventional phase diagrams using a new free energy minimization technique. The phase diagrams can be used to determine 1) bulk compositions and phase fields accessible by CVD techniques, 2) expected condensed phases for various starting gas mixtures and, 3) maximum equilibrium yields for specific CVD process variables. The three step thermodynamic method is used to calculate phase diagrams for the example CVD system Ti-B-Cl-H at 1200K and 800K. Examples of applications of the diagrams for yield optimization and experimental accessibility studies are presented and discussed. Experimental verification of the TiB_2 + Gas/Gas phase field boundary at 1200K, H/Cl = 1 confirms the calculated boundary and indicates that equilibrium is nearly and rapidly approached under laboratory conditions.

SAND80-0308

A SIMPLE METHOD FOR THE CALCULATION AND USE OF CVD PHASE DIAGRAMS WITH APPLICATIONS TO THE Ti-B-Cl-H SYSTEM, 1200K - 800K

INTRODUCTION

Chemical vapor deposition (CVD) is a process in which solid material is deposited from the chemical reaction or thermal decomposition of one or more gas species in the immediate vicinity of a solid substrate. CVD processes are used commercially to make a variety of materials including metals, nonmetals and refractory compounds.[1] Some common commercial CVD reactions are the deposition of Si by the H_2 reduction of $SiCl_4$ (as used by the semiconductor industry), the deposition of W by the H_2 reduction of WF_6, and the deposition of SiC from a mixture of H_2, CH_4 and $SiCl_4$. Pack cementation processes such as the boriding of steels are also CVD reactions. They are generally continuous processes with the reactant gases being mixed cold and then passed over a heated substrate where deposition occurs. Such reactions appear to involve rather simple chemical changes; however, the chemistry and atomic deposition mechanisms of CVD processes are complex. Gas phase mass transport, reaction kinetics, crystal growth and thermodynamic factors all play important roles.[1,2]

When analyzing a prospective CVD reaction, the first questions to be answered are: Is the reaction possible?. If so, what are the maximum yields to expect? What reactant gas composition should be used? Can the yield be improved by changing reactant gases? If the reaction is not possible, will a different choice of reactant gases make it possible? These questions can be answered by considering thermodynamic factors; therefore, a thermodynamic analysis should be the first step in analyzing any CVD reaction. Most CVD processes are continuous and there can be little doubt that at best they only approach equilibrium and under some conditions, not too closely. Nevertheless, thermodynamic (equilibrium) calculations have proven useful in predicting condensed phases in many CVD systems.[2-12]

In general, there are numerous gas and solid compounds present in a CVD system, and the chemical equilibria are quite complex. Historically, the early calculations considered free energy changes in only one simple reaction (See for example Ref. 11). Today, however, with the ever improving availability of thermochemical data and computational techniques, the problem of an equilibrium analysis of multicomponent, heterogeneous systems has become more tractable. Several authors have adopted existing computer codes for equilibrium calculations in various CVD systems,[2,3] but these codes tend to perform unpredictably and require users with considerable computer experience. A new and simpler computational procedure is presented below. This procedure is introduced with the goal of providing a powerful thermodynamic tool for the casual computer user.

A major problem with past studies has been the frequent practice of expressing the results of equilibrium calculations as "CVD phase diagrams." In these diagrams of which there are several forms, one or more atomic ratios are typically held constant in an effort to construct a two-variable diagram that is valid for systems of four or more components. Such diagrams hinder visualization of phase relationships for the system as a whole, and they often do not obey the Gibbs phase rule, thus making it difficult to interpret experimental data for CVD systems. The results obtained in the present study are presented systematically using true phase diagrams which obey the Gibbs phase rule.[14] In this way, experimental evidence can be presented to support the theoretical predictions of the positions of phase field boundaries. In addition to showing phase stability information, the phase diagrams are used to assess equilibrium yields and the feasibility of obtaining a desired phase(s), allowing that experimental restrictions are placed on CVD systems by the choice of input gases.

The computational and graphical procedures developed in this study are demonstrated with applications to the quaternary system Ti-B-Cl-H. Chemical vapor deposition in the Ti-B-Cl-H system is used for commercial production of the refractory, hard compound TiB_2 by the H_2 reduction of $TiCl_4$ and BCl_3.[11,13,15,16] The compound TiB_2 has many potential uses as a refractory material, for erosion and wear resistant coatings, and as an electrode coating for Hall-Heroult aluminum reduction cells.[17,18] Phase diagrams for this system are calculated at 1200K and 800K. Experimental verification using $TiCl_4$, BCl_3 and H_2 source gases is presented for important calculated phase boundaries at 1200K. Applications of the diagrams to practical problems, including experimental restrictions on source gases, are discussed.

EQULIBRIUM CALCULATION PROCEDURES

The method for CVD equilibrium calculations presented below proceeds in three steps: determination of equilibrium solid phase assemblages; evaluation of solid - gas stability relations; and calculation of phase diagrams. Examples from the Ti-B-Cl-H system at 1200K to 800K and 0.84 bar total pressure (8.4×10^4 Pa) illustrate each step of the procedure. The sources of the thermochemical data for the gas species and solid compounds considered in the calculations are summarized in Table 1. These data are almost identical to those used in a recent thermodynamic study of this system.[13]

Stable Solid Assemblages

Several solid compounds are typically present in systems of interest for CVD applications. Calculations of the standard Gibbs free energies of reactions over the temperature ranges of concern predict the individual compounds (assemblages) that are permitted in a thermodynamic sense. The stable solid assemblages for most CVD systems can usually be determined by consideration of a relatively small number of reactions. The standard Gibbs free energies for a set of fundamental reactions for solids in the Ti-B-Cl-H system at 1200K and 800K are given in Table 2.

TABLE 1

SOURCES OF THERMODYNAMIC DATA FOR CALCULATIONS IN THE Ti-B-Cl-H SYSTEM, 1200 to 800K

GAS SPECIES	SOURCE*	GAS SPECIES	SOURCE*
B	1	H	3
BCl	1	H_2	1
BCl_2	2	Ti	1
BCl_2H	1	TiCl	1
BCl_3	1	$TiCl_2$	1
BH	1	$TiCl_3$	1
BH_2	1	$TiCl_4$	1
BH_3	1		
B_2	1	SOLID	SOURCE*
B_2Cl_4	1	B	1
B_2H_6	1	Ti	1
B_5H_9	1	TiB	4
$B_{10}H_{14}$	1	TiB_2	5
Cl_2	1		
HCl	1		

*1. JANAF Thermochemical Tables 2nd Edition, D. R. Stull and H. Prophet eds., U.S. Government Printing Office, Washington, D.C. (1971).

2. JANAF Thermochemical Tables, 1974 Supplement, (1974).

3. JANAF Thermochemical Tables, 1975 Supplement, (1975).

4. Thermochemical Properties of Inorganic Substances, I. Barin and O. Knacke, Springer-Verlag, New York, NY (1973).

5. Thermochemical Properties of Inorganic Substances, Supplement, I. Barin, O. Knacke, and O. Kubaschewski, Springer-Verlag, (1977).

TABLE 2

GIBBS FREE ENERGIES OF REACTION FOR SOLID ASSEMBLAGES IN THE Ti-B-Cl-H SYSTEM, 1200K and 800K

REACTION*	$\Delta G^{o}_{RX,\ 1200K}$ (kcal)	$\Delta G^{o}_{RX,\ 800K}$ (kcal)
(1) $Ti + 2B = TiB_2$	-72.792	-72.991
(2) $Ti + B = TiB$	-37.338	-37.036
(3) $TiB + B = TiB_2$	-35.454	-35.956
(4) $TiB_2 + Ti = 2TiB$	-1.883	-1.080

*All Ti-Cl condensed phases are unstable at 1200K-800K.

The data in Table 2 indicate several important conclusions about solid-solid stability relations for the example system. The results for reactions (1) and (2) imply that TiB_2 and TiB are stable by themselves, and that Ti and B, while stable individually, are unstable in each others presence. The results for reactions (3) and (4) indicate that the assemblages TiB + B and TiB_2 + Ti are unstable, but that TiB_2 + B, TiB + Ti, and TiB_2 + TiB are stable assemblages.

From these elementary considerations, we would predict phase diagrams for the Ti-B-Cl-H system at 1200K-800K containing the following stable assemblages:

(1) B

(2) TiB_2 + B

(3) TiB_2

(4) TiB_2 + TiB

(5) TiB

(6) TiB + Ti

(7) Ti

Solid-Gas Stability Relations

The second step of the procedure is to examine the stability of the solid assemblages in the presence of a gas phase. This is accomplished by calculating equilibrium constants for solid-gas reactions over the temperature range of interest and expressing the results on stability diagrams showing the stability of solid assemblages with respect to fugacities (or partial pressures) of specified components. Techniques for construction of stability diagrams have been thoroughly discussed elsewhere and the calculations required are easily performed with a desk calculator.[19]

Stability diagrams for the example system at 1200K and 800K can be constructed in terms of fugacities f_{Ti} and f_B since B-Ti phases are the only stable solids. The results for calculations at 1200K are given in Figure 1 where stability limits for B, TiB_2, TiB, Ti, and a gas phase containing Ti and B components are expressed as functions of log f_{Ti} and log f_B. Fugacity constraints imposed by the assemblages

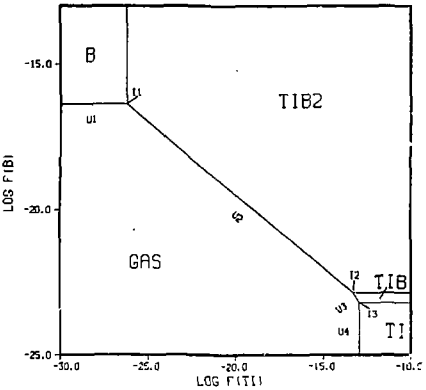

Fig. 1. Stability diagram for condensed Ti-B phases at 1200K.

B + TiB_2, TiB_2 + TiB, and TiB + Ti are represented by boundary lines between stability fields for the respective solid phases. The fugacity constraints corresponding to B + Gas (U_1), B + TiB_2 + Gas (I_1), TiB_2 + Gas (U_2), TiB_2 + TiB + Gas (I_2), TiB + Gas (U_3), TiB + Ti + Gas (I_3), and Ti + Gas (U_4) are of special interest in CVD applications and have been summarized in Table 3. The 800K stability diagram has a phase configuration and geometry similar to that of Figure 1; it can be constructed from the data in Table 3.

Calculation of Phase Diagrams

The above procedures provide a solution, albeit abstract, to the equilibrium problem frequently faced in CVD research. In a strictly thermodynamic sense Figure 1 is a phase diagram for solid-gas equilibrium. For practical purposes, however, a more practical expression of the phase relationships - especially those corresponding to U_1, U_2, U_3, U_4, I_1, I_2, and I_3 - in terms of bulk compositions in the Ti-B-Cl-H system would be desirable.

The qualitative character of a more practical phase diagram can be sketched from the results obtained in the above steps. This has been done in Figure 2 which shows an idealized section cut through the Ti-B-Cl-H tetrahedron at some fixed H/Cl ratio. Figure 2 can be constructed from a knowledge of the stoichiometry of the solid phases involved, the data presented above for stability relations, and the phase rule. For a four component system the phase rule (F = C - P + 2) at fixed temperature and pressure becomes

$$F = 4 - P \qquad (1)$$

TABLE 3

FUGACITY CONSTRAINTS FOR SOLID-GAS EQUILIBRIA
IN THE Ti-B-Cl-H SYSTEM AT 1200K and 800K

ASSEMBLAGE	EQUILIBRIA*
U_1: B + Gas	$B_{(c)} = B_{(g)}$ $\text{Log } f_B = -16.39_{(1200K)}, -28.49_{(800K)}$
U_2: TiB_2 + Gas	$TiB_{2(c)} = Ti_{(g)} + 2B_{(g)}$ $\text{Log } f_{Ti} + 2 \text{ Log } f_B = -58.98_{(1200K)}, -100.05_{(800K)}$
U_3: TiB + Gas	$TiB_{(c)} = Ti_{(g)} + B_{(g)}$ $\text{Log } f_{Ti} + \text{Log } f_B = -36.14_{(1200K)}, -61.74_{(800K)}$
U_4: Ti + Gas	$Ti_{(c)} = Ti_{(g)}$ $\text{Log } f_{Ti} = -12.94_{(1200K)}, -23.13_{(800K)}$
I_1: B + TiB_2 + Gas	$B_{(c)} = B_{(g)}$, $TiB_{2(c)} = Ti_{(g)} + 2B_{(g)}$ $\text{Log } f_B = -16.39_{(1200K)}, -28.49_{(800K)}$ $\text{Log } f_{Ti} = -26.20_{(1200K)}, -43.07_{(800K)}$
I_2: TiB_2 + TiB + Gas	$TiB_{2(c)} = Ti_{(g)} + 2B_{(g)}$, $TiB_{(c)} = Ti_{(g)} + B_{(g)}$ $\text{Log } f_{Ti} = -13.29_{(1200K)}, -23.42_{(800K)}$ $\text{Log } f_B = -22.85_{(1200K)}, -38.31_{(800K)}$
I_3: TiB + Ti + Gas	$TiB_{(c)} = Ti_{(g)} + B_{(g)}$, $Ti_{(c)} = Ti_{(g)}$ $\text{Log } f_{Ti} = -12.94_{(1200K)}, -23.13_{(800K)}$ $\text{Log } f_B = -23.19_{(1200K)}, -38.61_{(800K)}$

*All Data assume unit activity for solids.
c = condensed phase
g = gas species

where F is the number of degrees of freedom, C is the number of components (4), and P is the number of phases in an equilibrium assemblage. This expression applies to the tetrahedron but reduces to

$$F = 3 - P \qquad (2)$$

for a triangular section at fixed H/Cl, within which the effective number of components is reduced by one.

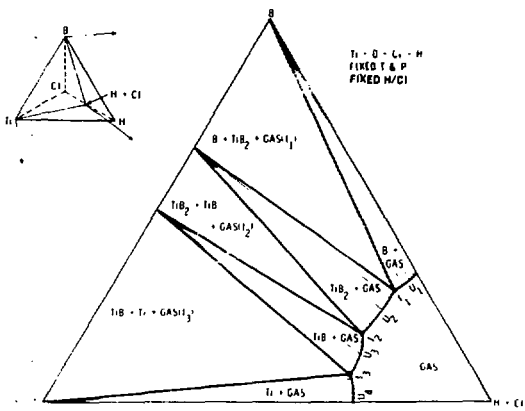

Fig. 2. Schematic section of the Ti-B-Cl-H quaternary phase diagram at fixed temperature, pressure, and H/Cl ratio.

The triangular section in Figure 2 is everywhere consistent with (2): the single phase Gas region corresponds to two degrees of freedom; the two-phase portions of the diagram (B + Gas, TiB_2 + Gas, TiB + Gas, and Ti + Gas) correspond to one degree of freedom represented by univariant gas compositions U_1, U_2,,U_3, U_4; and the three-phase portions of the diagram (B + TiB_2 + Gas, TiB_2 + TiB + Gas, and TiB + Ti + Gas) have zero degrees of freedom, corresponding to invariant compositions

I_1, I_2, and I_3. It should be noted that invariant and univariant conditions within a triangular section become respectively univariant and divariant within the tetrahedron.

It is clear that the simple calculations performed up to this point and incorporated via the phase rule in a diagram such as Figure 2 provide a very useful qualitative aid for visualizing the Ti-B-Cl-H system. Figure 2 indicates that a TiB_2 + Gas volume exists within the Ti-B-Cl-H tetrahedron and that it is bordered by assemblages containing B + TiB_2 + Gas, TiB_2 + TiB + Gas, and Gas. It is also evident that gas phase compositions for TiB_2 + Gas are less constrained than those of bordering assemblages. We do not know the precise location of the TiB_2 + Gas volume, but because sufficient thermochemical data for gaseous species in the Ti-B-Cl-H system are available, its location can be determined by methods described below. Even without the benefit of adequate thermochemical data, Figure 2 would greatly facilitate the experimental determination of the phase diagram at select H/Cl values.

Calculation of the positions of phase fields in Figure 2 requires determinations of bulk Ti-B-Cl-H gas compositions compatible with the constraints for U_1, U_2, U_3, U_4, I_1, I_2, and I_3 (Table 3) and lying on triangular sections at H/Cl values of interest. For these purposes, it is necessary to compute the equilibrium distributions of gaseous species in Ti-B-Cl-H mixtures as a function of temperature, pressure and H/Cl. Techniques for equilibrium calculations in CVD systems were recently reviewed by Spear.[2] He notes that numerous methods have been used but that all techniques are based on the earlier methods of Brinkley[20] or White et al.[21].

The method of Brinkley is based on equilibrium constants for dominant reaction equilibria at the bulk composition of interest. This approach requires simultaneous solution of non-linear equations, and it is difficult to formulate the method in a computer code that is sufficiently general to be applicable to different systems or to greatly different bulk compositions within the same system. The latter shortcomings often necessitate frequent rewriting of the code for each new system or bulk composition. The method of White et al. is a simple and direct free energy minimization technique that can easily be coded in a general manner applicable to any bulk composition in any chemical system of interest. It also has the advantage of reducing the problem to one of solving simultaneous linear equations.

The method of White et al. was originally developed for homogeneous gas phase equilibria calculations. Eriksson[22,23] extended the method to condensed phases including condensed solutions. SOLGASMIX, the computer program for the extended method, is relatively complicated for the casual computer user, and it requires substantially more core and time than do codes based on the initial method of White et al. for gas phase calculations alone. These additional complexities arise from involving condensed phases directly in the calculations. Unfortunately, most problems that are complicated enough to demand computerized thermodynamic calculation tend to be those involving multiphase equilibria.

To avoid the problems involved in treating condensed phases directly in the calculation, the original technique of White et al. could be used by starting at the H + Cl apex of a triangular section and calculating gas phase equilibria for progressively B - and Ti - richer bulk compositions. The equilibrium species distribution would

be calculated by free energy minimization at each bulk composition point subject to the constraints of temperature, total pressure, and mass of each elemental component implied by the bulk composition. The values of f_{Ti} and f_B would be noted at each step and compared with the values in Table 3. The critical bulk compositions corresponding to U_1, U_2, U_3, U_4, I_1, I_2, and I_3 could be obtained in this manner but only at the cost of considerable time and effort.

The critical compositions can be obtained precisely and directly using a method developed by the second author.[24] The method is an adaptation of that originally developed by White et al. for gas phase equilibrium calculations. A derivation of the method is given in the appendix. The essential feature of the technique is the option to replace one or more mass balance constraints with one or more fixed chemical potentials (or fugacities) for select species.

In the present system, appropriate values of f_{Ti} and f_B from Table 3 were used in place of mass balance constraints for Ti and B. The solutions obtained give the gas phase speciation consistent with temperature, pressure, H/Cl, f_{Ti}, and f_B chosen for the calculation. Bulk amounts of Ti and B are added or substracted during the calculations as required by the f_{Ti} and f_B constraints at the temperature, pressure and H/Cl of interest. Hence, the bulk gas compositions corresponding to U_1, U_2, U_3, U_4, I_1, I_2, and I_3 can be calculated directly and precisely from the critical fugacity data in Table 3. This method of calculation literally maps along the U_1, U_2, ... etc. curves in one sweep guided by f_{Ti} and f_B input data. The phase diagram is determined in an efficient manner without the complications and expense of treating condensed phases explicitly in the calculation.

Solid solutions can be handled by adjusting the fixed fugacities as required by the activities of components in the solids. Non-ideality in the gas phase is treated in the code by a corresponding state version of the Redlich - Kwong equation. This extra consideration proved unnecessary for the calculations reported here; it may, however, become necessary for calculations near critical points.

The calculation procedure described here has been coded to run on the CDC 6600 NOS time-sharing system at Sandia Laboratories. Equilibrium is generally obtained in 10 or less iterations regardless of initial values as long as the restrictions listed in the appendix are satisfied. The calculations for the phase diagrams presented below were carried out in a few hours in one afternoon. The rapid and convenient nature of the calculation procedure allows the user extra time for the worthwhile task of finding and evaluating thermochemical input data.

Ti-B-Cl-H PHASE DIAGRAMS

Phase diagrams for the Ti-B-Cl-H system were calculated at 1200K and 800K at our laboratory atmospheric pressure of 0.84 bar (8.4×10^4 Pa). Three triangular sections of the tetrahedron were plotted at each temperature: The Ti-B-Cl face, a section at H/Cl = 1.0 and the Ti-B-H face. These sections are shown in Figures 3a-e. The Ti-B-H face is for graphical purposes identical at 1200 and 800K. Values for I_1, I_2, and I_3 at 1200 and 800K are listed in Table 4. The transition is smooth between sections for different H/Cl ratios at constant temperature and pressure and intervening triangular sections can be interpolated. The B + Gas, TiB + Gas and Ti + Gas fields are extremely narrow bands. For practical CVD purposes, they can be ignored. The

TABLE 4

VALUES FOR I_1, I_2, I_3 IN THE Ti-B-Cl-H SYSTEM AT 0.84 BAR (8.4×10^4 Pa) (VALUES IN ATOMIC PERCENT)

		H/Cl RATIO		
		0	1	∞
(1200K)				
I_1	Ti	1.65×10^{-5}	5.25×10^{-6}	3.73×10^{-25}
	B	25.00	13.34	5.56×10^{-5}
	Cl	75.00	43.33	---
	H	---	43.33	100.00
I_2	Ti	24.29	13.92	3.07×10^{-2}
	B	1.64×10^{-11}	1.56×10^{-10}	1.94×10^{-11}
	Cl	75.71	43.04	---
	H	---	43.04	100.00
I_3	Ti	24.44	14.00	6.77×10^{-12}
	B	6.43×10^{-12}	4.33×10^{-11}	8.78×10^{-12}
	Cl	75.56	43.00	100.00
	H	---	43.00	---
(800K)				
I_1	Ti	2.41×10^{-7}	9.22×10^{-8}	3.73×10^{-25}
	B	25.00	14.36	5.56×10^{-5}
	Cl	75.00	42.82	---
	H	---	42.82	100.00
I_2	Ti	22.36	12.82	3.07×10^{-12}
	B	3.61×10^{-18}	2.06×10^{-16}	1.94×10^{-11}
	Cl	77.64	43.59	---
	H	---	43.59	100.00
I_3	Ti	22.61	12.97	6.77×10^{-12}
	B	1.02×10^{-18}	7.32×10^{-17}	8.78×10^{-12}
	Cl	77.39	43.51	100.00
	H	---	43.51	---

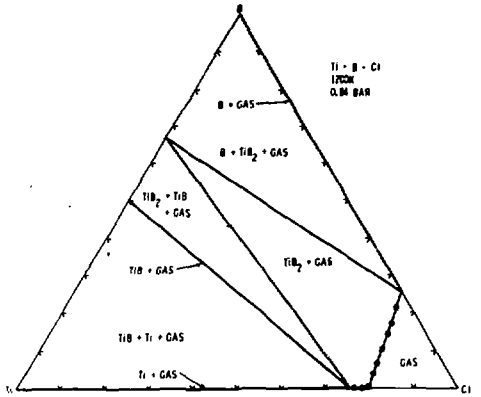

a

Fig. 3. Calculated Ti-B-Cl-H phase diagrams at 0.84 bar total pressure. a) 1200K, H/Cl = 0, b) 1200K, H/Cl = 1, c) 1200 and 800K, H/Cl = ∞, d) 800K, H/Cl = 0, e) 800K, H/Cl = 1. Axes are marked at 10% intervals. Filled circles indicate calculated points on U2.

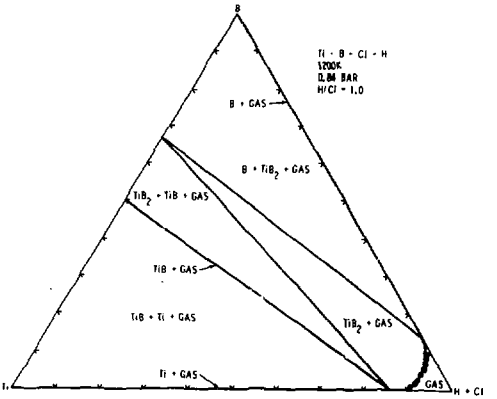

b

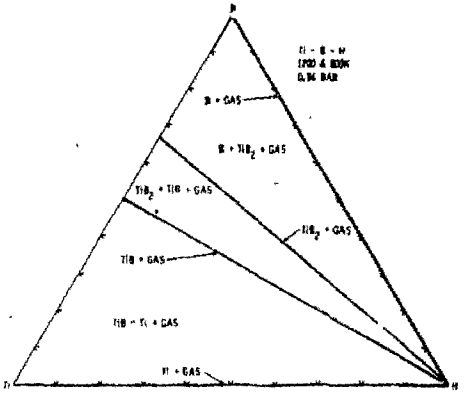
B
Ti - B - H
1200 K 800K
0.84 BAR
B + GAS
B + TiB2 + GAS
TiB2 + TiB + GAS
TiB2 + GAS
TiB + GAS
TiB + Ti + GAS
Ti + GAS
Ti
H

c

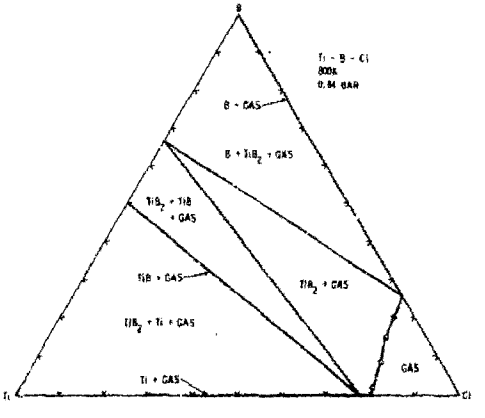
B
Ti - B - Cl
800K
0.84 BAR
B + GAS
B + TiB2 + GAS
TiB2 + TiB
+ GAS
TiB + GAS
TiB2 + GAS
TiB2 + Ti + GAS
GAS
Ti + GAS
Ti
Cl

d

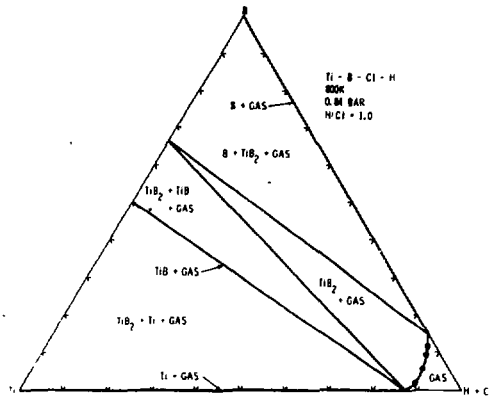

e

TiB_2 + Gas field is the main phase field of interest since TiB_2 is the desired condensed phase and a schematic three dimensional view of this field at 1200K is shown in Figure 4. On the Ti-B-Cl face, it is roughly

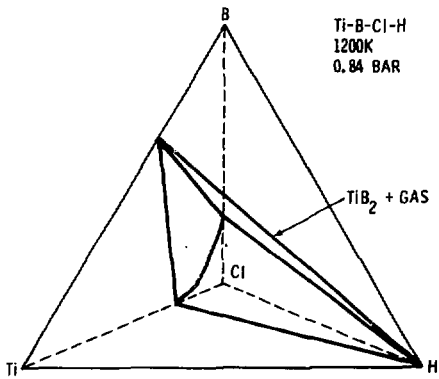

Fig. 4. TiB_2 + Gas phase field at 1200K.

triangular in shape (Figure 3a) and at higher H/Cl ratios it becomes narrower and converges to a line on the Ti-B-H face of the tetrahedron (Figure 3c). The TiB_2 + Gas field behaves in the same manner at 800K (Figure 3c-e). The only difference is a slight curvature change in the TiB_2 + Gas/Gas phase field boundary (U_2).

GAS SPECIES ALONG THE TiB_2 + GAS/GAS PHASE BOUNDARY IN THE Ti-B-Cl-H SYSTEM

Figure 5 illustrates speciation in the gas phase of the TiB_2 + Gas portion of the 1200K phase diagram at H/Cl = 1. The speciation is expressed as log partial pressures of the main species in gases with a range of bulk compositions identified by filled circles on the calculated TiB_2 + Gas/Gas boundary in Figure 3b. The bulk compositions are expressed as log B/Ti in Figure 5. The calculations included all 22 gas species listed in Table 1 but only those with partial pressures greater than 10^{-4} bar (10 Pa) are shown in Figure 5.

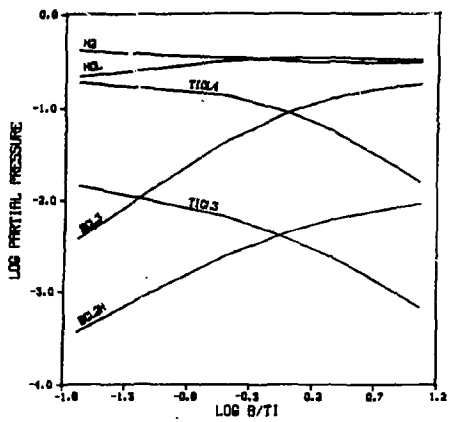

Fig. 5. Calculated partial pressures of major gas species along the 1200K TiB_2 + Gas/Gas boundary for H/Cl = 1 (U_2 in Figure 3b).

The trends shown in Figure 5 continue at higher and lower B/Ti approaching I_1 and I_2 respectively. At I_1, the gas phase consist almost entirely of H_2, HCl, BCl_3, and BCl_2H; all Ti-species approach zero concentrations. At low B/Ti, near I_2, the gas phase is predominantly $TiCl_4$, $TiCl_3$, H_2, and HCl.

The major gas species along the TiB_2/Gas boundary at 1200K for H/Cl = 1 (Figure 3b) are BCl_3, BCl_2H, $TiCl_4$, $TiCl_3$, HCl, and H_2 (Figure 5). All other species are of minor significance. As H/Cl increases and the Ti-B-H face of the tetrahedron (Figure 2) is approached, all Cl-containing species (including those of Ti) decrease, and the major species become BH_2, BH_3, and H_2 with minor B_2H_6, B_5H_9, $B_{10}H_{14}$, BH, B_2, and H. Gases become progressively depleted in Ti as H/Cl increases. At lower H/Cl near the Ti-B-Cl face, H-containing species become increasingly unimportant, and the major species are BCl_3, B_2Cl_4, BCl_2, $TiCl_4$, $TiCl_3$, and $TiCl_2$ with minor and trace Cl_2, BCl, B_2, TiCl, and B.

The gas speciation patterns summarized above for 1200K remain essentially unchanged at 800K. Figure 5 redrawn for 800K shows the same major species in the same relative amounts.

EXPERIMENTAL VERIFICATION

The calculated Ti-B-Cl-H phase diagram shows that Ti, TiB, TiB_2 and B are all stable as condensed phases at 1200K and 800K for appropriate bulk compositions. As will be discussed later, not all of the phase fields on the diagram can be attained by the experimentalist. For this reason, the only condensed phases possible in practice are TiB_2 and B; and B is condensed only at very high B/Ti ratios. In fact, the only phase boundary which can be experimentally determined

accurately is the TiB_2 + Gas/Gas boundary (U_2). Therefore, an attempt was made to determine the position of this boundary at 1200K and H/Cl = 1.

Procedure

The CVD reactor used was a 6.5 cm x 37 cm long fused silica tube and has been described in detail elsewhere.[15,16] The reactant gases $TiCl_4$, BCl_3, H_2 and HCl were preheated to 573K by passage through a mixing chamber before being brought into the reactor. The substrate was heated with an RF generator and temperature was controlled at 1200 $\pm$ 5K with a type S thermocouple inserted into the susceptor. Both substrates (2.5 cm x 3 mm discs) and susceptor were Poco AXF-5Q graphite. Gas flow rates were measured with Teledyne-Hastings mass flow meters and were repeatable with a minimum precision of $\pm$ 5% relative. $TiCl_4$ was metered with a Sage 220 syringe pump which had a measured accuracy of $\pm$ 2%. Total run time, defined as the actual flow time of reactant gases, was 20 minutes. The total gas flow rate was 500 ml/m or less. The reactants were used as received without further purification or drying. The stated purity levels were: $TiCl_4 \geq 99.$..8, $BCl_3 \geq 99.9\%$, $H_2 \geq 99.999\%$ and HCl $\geq 99.0\%$.

The presence of a TiB_2 coating was detected using visual, x-ray diffraction and weight gain measurement techniques. Weight gain proved to be the most useful of these techniques. Weighing precision was determined to be $\pm$ 0.0005 gm by making several runs using only H_2 and/or HCl as input gases. A conservative detectability limit was, therefore, chosen as 0.001 gm and weight gains less than this were ignored.

Results

The TiB_2 + Gas/Gas boundary as determined at 1200K, 0.84 bar (8.4×10^4 Pa), and H/Cl = 1 is shown in Figure 6. Filled circles represent CVD conditions where single phase (as determined by x-ray diffraction) TiB_2 was obtained. Unfilled circles represent conditions where no deposit was obtained. The calculated boundary (U_2) is shown on the diagram as a solid line. The small filled circles on the line represent actual calculated points. The agreement between the experimental and calculated boundary is excellent. The experimental boundary may be located slightly to the left of the calculated boundary but this shift could be no more than ~1% HCl (See Figure 6).

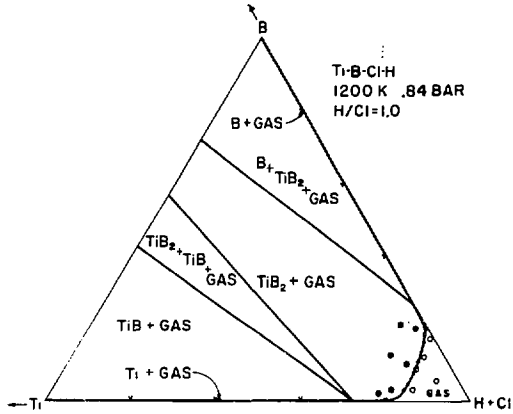

Fig. 6. Experimental verification of the calculated TiB_2 + Gas/Gas boundary (U_2). Large filled circles represent CVD conditions where TiB_2 deposits were observed, unfilled circles represent conditions where no deposits were observed. Smaller dots correspond to calculated points along U_2 in Figure 3b.

Since this experimental system is not a closed system, the most likely cause of the minor disagreement between theory and experiment is reaction kinetics. The open or flowing system obviously approaches but does not reach equilibrium. As the Gas field boundary is approached in the TiB_2 + Gas field, supersaturation of TiB_2 approaches zero and the deposition rate also approaches zero. Precise determination of the phase boundary would, therefore, require very long reaction times and very low flow rates or a closed system experiment. Since the purpose of presenting the method is for practical applications, realistic CVD conditions were used. The results indicate that not only are the thermodynamic calculations correct, but they are applicable to actual CVD conditions. This experimental determination, to the best of the authors' knowledge, represents the first time the position of a calculated phase field boundary has been unquestionably verified for a four component CVD system.

APPLICATION OF THE PHASE DIAGRAMS

Yield Estimation

The calculated diagrams as presented in Figure 4, can be applied in several ways. Since they are true phase diagrams, tie lines lie in the plane of the diagram and equilibrium or theoretical yields can be obtained in a straightforward manner by constructing a tie line through the reactant gas bulk composition.[14] Examples of tie line construction are illustrated for two phase regions in Figure 2. The endpoints of the tie line give the gas and solid compositions at equilibrium, and a simple application of the lever rule gives the equilibrium yield of the product, TiB_2. No other yield calculations are necessary as with previous other types of "CVD phase diagrams."[2] This graphical method

can be used to calculate equilibrium yields, e.g., the maximum theoretical efficiency for any bulk reactant gas mixture.

Experimental Accessibility

A second and more useful application of the diagrams is as an aid in the understanding of experimental restrictions on the CVD system. Given a certain set of input gases, it may not be possible to operate experimentally in all of the phase fields of the diagram. For example, consider the H_2 reduction of $TiCl_4$ and BCl_3. In this case, $TiCl_4$ and BCl_3 are the Ti and B source gases and the CVD experimentalist is restricted to a small region of the Ti-B-Cl-H tetrahedron bounded by the Cl-H edge. The experimentally accessible volume of the Ti-B-Cl-H tetrahedron is a three sided pyramid as shown schematically in Figure 7. To visualize this, consider the diagram shown in Figure 8. On the Ti-B-Cl face, (H/Cl = 0) the experimentalist cannot have conditions more rich in Ti than pure $TiCl_4$ (80% Cl). Similarly, he cannot have conditions more rich in B than pure BCl_3 (75% Cl). He can operate between these two points by varying the $BCl_3/TiCl_4$ ratio and this limit is shown by a line running between $TiCl_4$ and BCl_3 (H/Cl ratio = 0 on Figure 8). The area to the right of this line (as shown by the arrows) is accessible by adding Cl_2 to the system (remember H/Cl = 0 so there is no H_2 in this example). The major portion of the diagram to the left of this line is inaccessible to the experimentalist with the given source gases. Similar accessible areas can be calculated when H_2 is present, e.g., at different H/Cl ratios, and plotted. Those for H/Cl ratios of one, five and infinity are shown in Figure 8. As H/Cl increases, the accessible area becomes smaller and comes to a point at H/Cl >>1 e.g., on the Ti-B-H face of the tetrahedron.

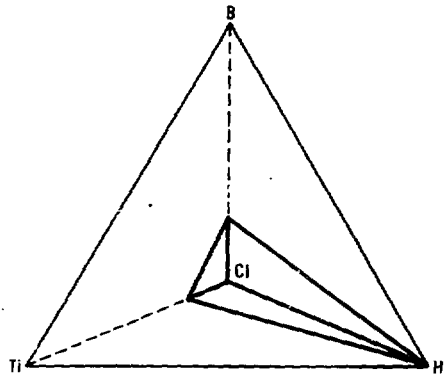

Fig. 7. Accessible volume of the Ti-B-Cl-H system for $TiCl_4$ and BCl_3 source gases.

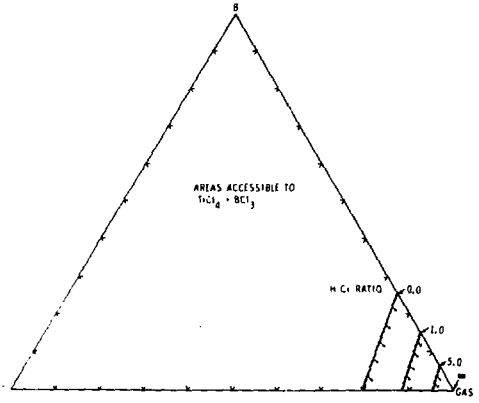

Fig. 8. Accessible areas of the Ti-B-Cl-H system for $TiCl_4$ and BCl_3 sources gases at H/Cl = 0, 1, 5, ∞.

The benefits of this accessibility approach can be demonstrated by overlaying the accessibility diagram on the phase diagram. An example is shown in Figure 9 for H/Cl = 1 at 1200K. Line PQ represents the boundary of the accessible area. The boundary of the TiB_2 + Gas phase field is shown by a dotted line. If BCl_3 and $TiCl_4$ ratios are chosen such that B/Ti = 1 (and sufficient H_2 is added to reach H/Cl = 1) point 0 is the CVD operating point or bulk reactant gas composition. This point lies well inside the TiB_2 + Gas field and should produce TiB_2 under equilibrium conditions. Movement along line PQ is accomplished by varying the $BCl_3/TiCl_4$ ratio (and hence the B/Ti ratio) and movement to the right of 0 is accomplished by adding gas (H + Cl) which has H/Cl equal to one. By adding enough gas, it is possible to enter the Gas single phase field where no deposition of TiB_2 will occur. This was the method used to verify this boundary in the previous section. Tie line construction and the lever rule will predict efficiency for any point 0 in a multiphase field.

Overlaying the accessibility and phase diagrams at 1200K for various H/Cl ratios indicates that it is not thermodynamically possible to obtain Ti or TiB using $TiCl_4$ and BCl_3 source gases. It is possible to enter the B + TiB_2 + Gas field, however, at some H/Cl ratios for very high B/Ti ratios (See Figure 9). Unfortunately, for the experimentalist, the overlap is very small and theoretical efficiencies would be very low. It is doubtful that much if any B would be co-deposited with TiB_2.

Other information contained in the diagram includes which B/Ti ratios to use for higher thermodynamic yields. As tie line construction will show for the various bulk reactant gas compositions in

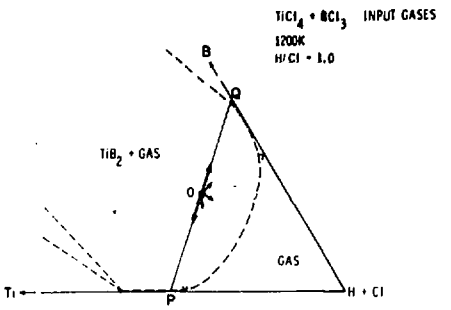

Fig. 9. Superposition of the phase diagram and accessibility diagram for $TiCl_4$ and BCl_3 source gases at 1200K, H/Cl = 1.

Figure 9, high or low B/Ti ratios would not be desirable since the operating point more closely approaches the TiB_2 + Gas/Gas boundary. Similarly adding HCl will decrease yields. Comparing the diagrams for 1200K and 800K, it can be seen that increased yields should be obtained at 1200K due to the increased curvature of TiB_2 + Gas/Gas boundary at 1200K.

Optimizing Yield and Accessibility

Temperature does not affect the basic geometry of the phase diagram to a large extent in the 800-1200K temperature range but system chemistry does. In particular, the H/Cl ratio is quite effective in changing the shape of the TiB_2 + Gas phase field. Therefore, to the experimentalist chemistry would be the first choice to optimize the system. Unfortunately, for $TiCl_4$, BCl_3 and H_2 source gases, the accessible area changes with the H/Cl ratio as well (Figure 8) and it literally follows the change in the TiB_2 + Gas/Gas boundary; thus

after a point increasing H/Cl while maintaining $TiCl_4$, BCl_3 and H_2 as source gases does not increase the theoretical yield.

There are other methods to accomplish substantial yield increases. For example, other source gases are available such as B_2H_6. The accessible areas of the diagram using $TiCl_4$ and B_2H_6 as source gases (and H_2 and Cl_2 as diluents) are shown in Figures 10 and 11. Both the shape and the extent of the accessible area have changed. The accessible area at 1200K and H/Cl = 1 is as shown in Figure 12. Point 0 is the operating point for pure $TiCl_4$ and B_2H_6 (e.g., B/Ti = 1.33). The area to the right of 0 (as shown by the small arrows) is again accessible by adding H + Cl. Note that with $TiCl_4$ and B_2H_6 source gases the movement restrictions on 0 are different from those of Figure 9. Point 0 cannot move along PQ unless the H/Cl ratio changes and, of course, the shape of the TiB_2 + Gas field will change accordingly. Comparing the position of 0 in Figures 9 and 12 and applying the lever rule, it can be seen that using B_2H_6 as a B source increases the equilibrium yield substantially. At 1200K and H/Cl = 1, the optimum operating point for both BCl_3 and B_2H_6 B source gases is B/Ti ~1.33. Under these conditions, using B_2H_6 would result in a yield increase of ~330% over BCl_3. Such large yield gains have been experimentally noted by other investigators.[25]

CONCLUSIONS

The procedures discussed above provide a simple and direct method for calculating and displaying equilibrium relationships in relatively complex CVD systems. The efficient and systematic nature of the method allows a comprehensive examination of the entire chemical system of interest. Graphical display of the results on phase diagrams which

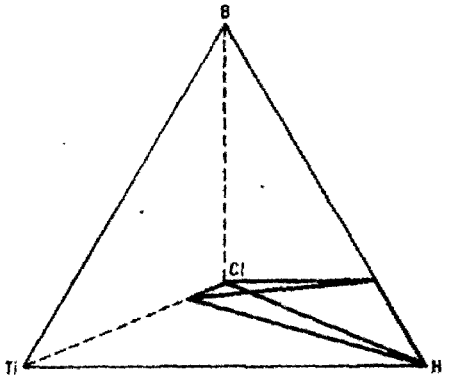

Fig. 10. Accessible volume of the Ti-B-Cl-H system for $TiCl_4$ and B_2H_6 source gases.

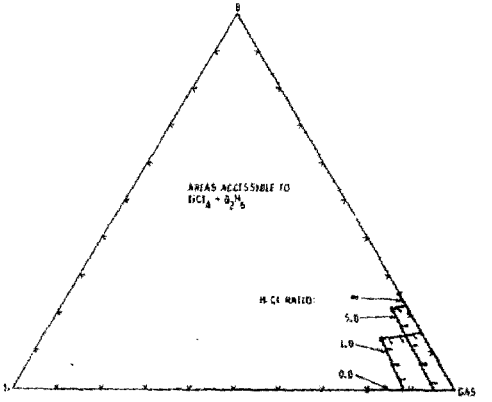

Fig. 11. Accessible areas of the Ti-B-Cl-H system for $TiCl_4$ and B_2H_6 source gases at H/Cl = 0, 1, 5, ∞.

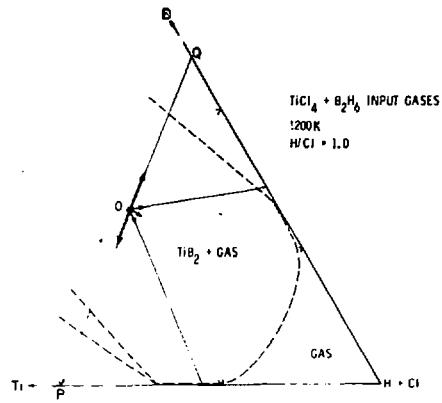

Fig. 12. Superposition of the phase diagram and accessibility diagram for $TiCl_4$ and B_2H_6 source gases at 1200K, H/Cl = 1

obey the phase rule provide a powerful tool for guiding experimental studies, interpreting experimental data, evaluating potential CVD source gases for optimal yields, and appraising the feasibility of depositing compounds that have not been investigated empirically by CVD techniques.

The results for the Ti-B-Cl-H system suggest that phase relationships are far more sensitive to changes in system chemistry than they are to changes in temperature. It would be of interest to determine if this generalization is also true for other CVD systems and for other temperatures outside the range employed in this study. The results for the Ti-B-Cl-H system also suggest that equilibrium is closely approached under typical CVD conditions for TiB_2 deposition. Hence, thermodynamic studies have significant predictive value for this CVD system.

ACKNOWLEDGEMENTS

The authors' wish to thank N. G. Benton for her help with the CVD experimentation.

REFERENCES

1. Vapor Deposition, C. F. Powell, J. H. Oxley, J. M. Blocher, Jr., ed., John Wiley and Sons, Inc. The Electrochemical Society, Princeton, NJ (1966).

2. K. E. Spear, "Applications of Phase Diagrams and Thermodynamics to CVD." Proc. Seventh International Conference on CVD, T. O. Sedgewick and H. Lydtin, ed., Electrochem. Society, Princeton, NJ (1979) 1.

3. C. Bernard, Y. Demil, A. Jacquot, P. Vay, and M. Ducarroir, "Détermination des Equilibres Chimques Complexes dans les Systemés Polyphasés." J. Less Common Metals, 40 (1975) 165-171.

4. R. L. Gentilman, "Chemical Vapor Deposition of Epitaxial Films of Yttrium Iron Garnet and Gallium-Substituted Yttrium Iron Garnet and a Thermodynamic Analysis." J. Amer. Cer. Soc., 56, 12, (1973) 623-7.

5. P. N. Walsh, "Equilibrium Chemistry of Boron Deposition." Proc. Fourth International Conference on CVD, 1973. G. F. Wakefield and J. M. Blocher, Jr., eds., The Electrochemical Society, Princeton, NJ, (1973) 135-43.

6. S. Minagawa, and H. Seki, "Thermodynamic Analysis of the Vapor Growth of $Al_x Ga_{1-x}As$: The Al-Ga-As-Cl-H System." Proc. Fourth International Conference on CVD, 1973. G. F. Wakefield and J. M. Blocher, Jr., eds., The Electrochemical Society, Princeton, NJ (1973) 50-62.

7. J. J. Nickl, K. K. Schweitzer, and P. Luxenberg, "Chemical Vapor Deposition of the Systems Ti-Si-C and Ti-Ge-C." The Third International Conference on Chemical Vapor Deposition. F. A. Glaski ed., American Nuclear Society, Hinsdale, Illinois (1973), 4-23.

8. R. W. Haskell, "Absolute Reaction Rate Theory Applied to Tungsten Deposition via Reduction of the Hexafluoride." Proc. Second International Conference on CVD. J. M. Blocher, Jr., and J. C. Withers eds., The Electrochemical Society, New York, (1970) 63-70.

9. J. E. Carlton, J. H. Oxley, E. H. Hall, and J. M. Blocher, Jr., MKinetics of the Hydrogen Reduction of Boron Trichloride to Boron." Proc. Second International Conference on CVD. J. M. Blocher, Jr., and J. C. Withers eds., The Electrochemical Society, New York (1970) 209-26.

10. S. E. Bradshaw, "The Kinetics of Epitaxial Silicon Deposition by the Hydrogen Reduction of Chlrosilanes." Int. J. Electronics, 21, 3, (1966) 205-27.

11. P. Peshev, and T. Niemyski, "Préparation de Diborure de Titane Cristallin au moyen d'une Réaction en Phase Gazeuse." J. Less Common Metals, 10, (1965) 133-45.

12. T. O. Sedgwick, "Analysis of the Hydrogen Reduction of Silicon Tetrachloride Process on the Basis of a Quasi-Equilibrium MOdel." J. Electrochemical Society, 111 12, (1964) 1381-3.

13. T. M. Besmann and K. E. Spear, "Analysis of the Chemical Vapor Deposition of Titanium Diboride I. Equilibrium Thermodynamic Analysis." J. Electrochemical Society, 124, (1977) 786-790.

14. Phase Diagrams in Metallurgy, F. N. Rhines, McGraw-Hill Book Co. (1956).

15. H. O. Pierson and E. Randich, "The Coating of Materials with TiB_2 by Chemical Vapor Deposition." Proc. Sixth International Conference on CVD, L. G. Donaghey and P. Rai-Chandbury ed., The Electrochemical Society, NY, (1977), 304-317.

16. H. O. Pierson and E. Randich, "Titanium Diboride Coatings and their Interaction with the Substrates." Thin Solid Films, 54, (1978) 119-125.

17. L. Kaufman and E. V. Clougherty in "Plansee Proceedings, 1964," (Metals for the Space Age), Metallwerk Plansee AG, Reutte/Tirol (1965) 722-758.

18. See for example: U.S. Patent 3,400,061, R. A. Lewis and R. D. Hilderbrandt (1968) or United Kingdom Patent 802,905 C. E. Ransley, (1958).

19. Introduction to Metallurgical Thermodynamics, D. R. Gaskill, McGraw-Hill Book Co., New York, NY (1973).

20. S. R. Brinkley, Jr., "Calculation of the Equilibrium Composition of Systems of Many Constituents." J. Chem. Phys. 15, 2, 107-110.

21. W. B. White, S. M. Johnson, and G. B. Dantzig, "Chemical Equilibrium in Complex Mixtures." J. Chem. Physics, 28, 5 (1958) 751-755.

22. G. Eriksson, "Thermodynamic Studies of High Temperature Equilibria. III SOLGAS, a Computer Program for Calculating the Composition of an Equilibrium Mixture." Acta Chem. Scand., 25 7, 2651-2658.

23. G. Eriksson, "Thermodynamic Studies of High Temperature Equilibria. XII SOLGASMIX, a Computer Program for Calculation of Equilibrium Compositions in Multiphase Systems." Chem. Scripta 8, (1975), 100-103.

24. T. M. Gerlach, in preparation.

25. H. O. Pierson, personal communication, (1980).

APPENDIX

The gas phase equilibrium distributions reported in this study were calculated subject to constraints on temperature (T), total pressure (P), element mass balances (b_1, b_2, ..., b_M), and chemical potentials (μ_1, μ_2, ..., μ_N). The method of computation is an adaptation of the free energy minimization technique of White et al.,[20] which was developed for problems where a full set of element mass balances is in force. The adaptation is applicable when one or more chemical potential (or fugacity) constraints replace one or more element mass balances.

In the mass balance constrained formulation of White et al.,[20] the free energy minimization of a perfect gas mixture* of M elemental components containing N species leads to a symmetric set of M + 1 linear equations in the M + 1 unknowns Π_1, Π_2, ..., Π_M, and U:

$$
\begin{aligned}
r_{11}\Pi_1 + r_{12}\Pi_2 + \ldots + r_{1M}\Pi_M + b_1 U &= \sum_{i=1}^{N} a_{i,1} g_i(m) \\
&\vdots \\
r_{1M}\Pi_1 + r_{2M}\Pi_2 + \ldots + r_{MM}\Pi_M + b_M U &= \sum_{i=1}^{N} a_{i,M} g_i(m) \\
b_1\Pi_1 + b_2\Pi_2 + \ldots + b_M\Pi_M + 0 \cdot U &= \sum_{i=1}^{N} g_i(m)
\end{aligned}
\qquad (1)
$$

*The derivation given here is for a perfect gas mixture in which each gas species of the mixture obeys the ideal gas equation of state. This procedure is followed for convenience only. Real gas behavior can easily be incorporated into the derivation by substituting appropriate fugacity-partial pressure relationships into (3) and (4).

where:

(a) m is a set of approximate equilibrium molar quantities for species i through N (i.e., m_1, m_2, ..., m_N).

(b) the total Gibbs free energy for the ith species is

$$g_i(m) = m_i \ (\mu_i/RT). \tag{2}$$

Note that μ_i/RT for a gas mixture can be expressed

$$\mu_i/RT = \mu_i^o/RT + \ln f_i \tag{3}$$

where f_i is the fugacity of i, μ_i^o is the standard Gibbs energy for i, and R is the universal gas constant. The fugacity of i in a perfect gas mixture may be taken as the partial pressure (p_i) from which it follows that

$$f_i = (m_i/\bar{m}) \ P \tag{4}$$

where

$$\bar{m} = \sum_{i=1}^{N} m_i. \tag{5}$$

Substituting (4) into (3) gives

$$\mu_i/RT = C_i + \ln \ (m_i/\bar{m}) \tag{6}$$

where

$$C_i \equiv \mu_i^o/RT + \ln P. \tag{7}$$

Hence (2) may be rewritten in terms of m:

$$g_i(m) = m_i \left[C_i + \ln m_i/\bar{m}\right]. \tag{8}$$

(c) a_{ij} is the stoichiometric coefficient defining the number of atoms of element j in species i.

(d) b_j is the mass balance constraint for element j:

$$b_j = \sum_{i=1}^{N} a_{ij} m_i. \tag{9}$$

(e) r_{jk} is a constant defined by

$$r_{jk} \equiv \sum_{i=1}^{N} (a_{ij} a_{ik}) m_i = r_{kj} \quad ; \; j,k = 1, \ldots, M. \tag{10}$$

(f) $\Pi_1, \Pi_2, \ldots, \Pi_M$ are the Lagrange undetermined multipliers.

(g) U is defined by

$$U \equiv (\bar{n}/\bar{m}) - 1 \tag{11}$$

where $\bar{n}$ is defined analogously to (5) and n is the set of improved molar quantities $(n_1, n_2, \ldots, n_N)$.

The symmetric set of linear equations (1) is solved to obtain $\Pi_1, \Pi_2, \ldots, \Pi_M$, and U. These values and (8) are used to obtain an improved set of molar quantities from

$$n_i = -g_i(m) + (\bar{n}/\bar{m}) m_i + \sum_{j=1}^{M} a_{ij} \Pi_j \, m_i, \tag{12}$$

which was derived by White et al.[20]

The improved set (n) is then used as the set of approximate equilibrium molar quantities (m) for the next iteration by calculating

(8) and (10), substituting into (1), and solving for new values of Π_1, Π_2, ..., Π_M, and U. This procedure is repeated until the difference between n and m satisfies a specified convergence criteria. The final set n gives the molar amounts of each species at equilibrium subject to a full set of mass balance constraints.

When one or more element mass balance constraints is replaced by one or more fixed chemical potentials, the symmetric set of linear equations in (1) is altered. Dropping a constraint such as (9) in effect removes an equation of the form

$$r_{jk}\Pi_j + r_{j\ell}\Pi_\ell + \ldots + r_{jM}\Pi_M + b_j U = \sum_{i=1}^{N} a_{ij} g_i(m) \qquad (13)$$

from (1).

At equilibrium, (12) becomes

$$\sum_{j=1}^{M} a_{ij}\Pi_j = \frac{g_i(n)}{n_i}$$

which with (8) and (6) gives

$$\sum_{j=1}^{M} a_{ij}\Pi_j = c_i + \ln n_i/\bar{n} = \mu_i/RT \qquad (14)$$

Hence, a linear equation with unknowns Π_1, Π_2, ..., Π_M is obtained by fixing the chemical potential (or fugacity) of a species. For example, fixing the chemical potential of species s (μ_s/RT = constant) gives

$$a_{s1}\Pi_1 + a_{s2}\Pi_2 + \ldots + a_{sM}\Pi_M = \mu_s/RT \qquad (15)$$

Replacing element mass balance constraints (9) with fixed chemical potentials (or fugacities) implies equations of the form (15) replace equations such as (13) in (1). The new symmetric matrix becomes

$$
\begin{aligned}
& r_{11}\Pi_1 + r_{12}\Pi_2 + \cdots + r_{1M}\Pi_M + b_1 U = \sum_{i=1}^{N} a_{i,1} g_i(m) \\
& \quad \vdots \qquad\quad \vdots \qquad\quad \vdots \qquad\quad \vdots \qquad\quad \vdots \\
& r_{1\ell}\Pi_1 + r_{2\ell}\Pi_2 + \cdots + r_{M\ell}\Pi_M + b_\ell U = \sum_{i=1}^{N} a_{i,\ell} g_i(m) \qquad (16) \\
& a_{s1}\Pi_1 + a_{s2}\Pi_2 + \cdots + a_{sM}\Pi_M + 0 \cdot U = \mu_s/RT \\
& \quad \vdots \qquad\quad \vdots \qquad\quad \vdots \qquad\quad \vdots \qquad\quad \vdots \\
& a_{s'1}\Pi_1 + a_{s'2}\Pi_2 + \cdots + a_{s'M}\Pi_M + 0 \cdot U = \mu_{s'}/RT \\
& b_1\Pi_1 + b_2\Pi_2 + \cdots + b_M\Pi_M + 0 \cdot U = \sum_{i=1}^{N} g_i(m).
\end{aligned}
$$

Equations (16), like (1), are solved for Π_1, Π_2, ..., Π_M, and U. These values are used to obtain a new set n from (12). The improved set is used in (16) on the next iteration, and the procedure is repeated until n and m converge. The final set n will be an equilibrium distribution satisfying the element mass balances retained and the fixed chemical potentials. The masses of elements for which mass balance constraints were discarded can now be calculated from n using equations analogous to (9).

The following precautions must be followed to avoid problems in applying this procedure:

(a) Chemical potentials must not be set at values which are impossible to achieve in the equilibrium gas at the T and P of interest.

(b) The specified chemical potentials must be independent of each other. For example, if μ_{O_2} and μ_{H_2O} are fixed, μ_{H_2} can not also be arbitrarily specified because of the reaction relation between O_2, H_2O, and H_2.

(c) The number of chemical potentials that may be arbitrarily specified is limited, of course, by the phase rule.